ECE 796:

Models of the Neuron

Slides for Lecture #8

Monday, March 9, 2009

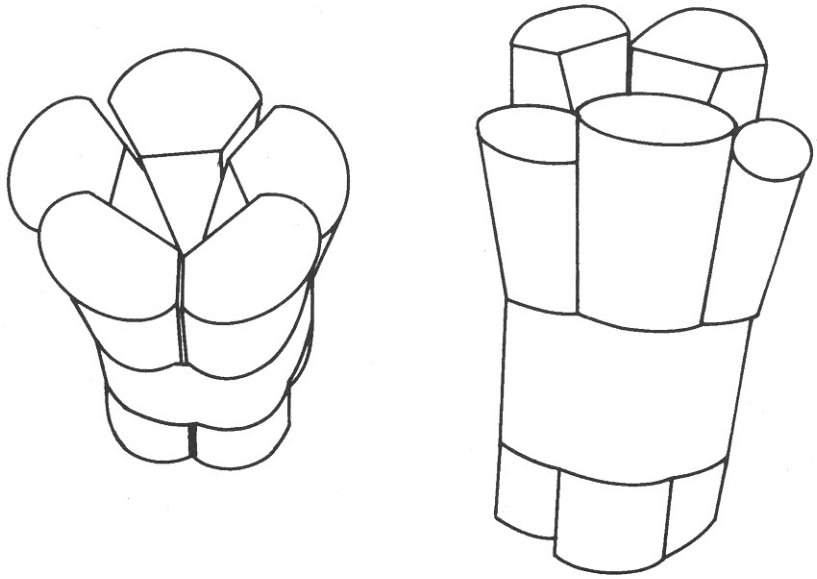

Figure 4.1. A model of the acetylcholine receptor which shows the five component subunits and the aqueous pore. The band locates the membrane bilayers through which the molecule passes; the lower part is cytoplasmic. [From R. M. Stroud and J. Finer-Moore, Acetylcholine receptor structure, function, and evolution. Reproduced with permission from *Annu. Rev. Cell Biol.* **1**:317–351 (1985). Copyright 1985, Annual Reviews, Inc.]

(from Plonsey
and Barr)

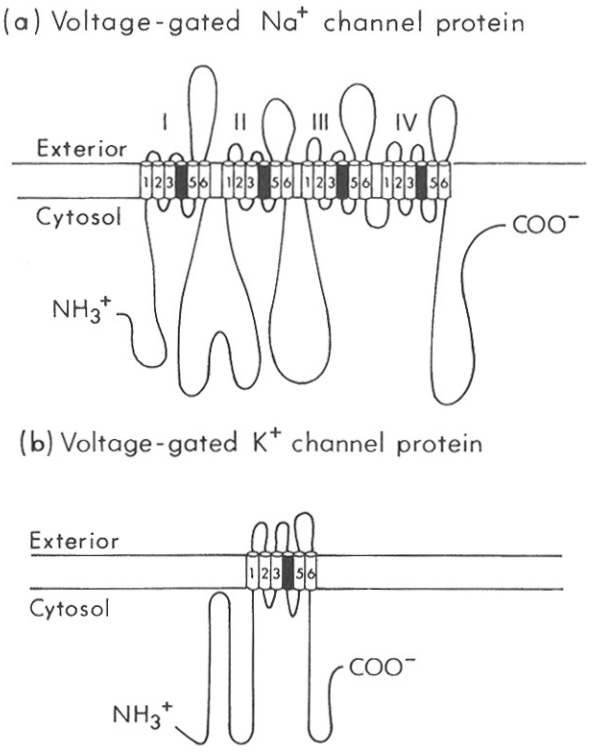

(from Plonsey and Barr)

Figure 4.2. Proposed transmembrane structure of (a) voltage-gated Na^+ channel protein and (b) voltage-gated K^+ channel protein. The sodium channel arises from a single gene; it contains 1800–2000 amino acids, depending on the source. About 29 percent of the residues are identical to those in the voltage-gated Ca^{++} channel protein. There are four homologous domains indicated by the Roman numerals. Each of these is thought to contain six transmembrane α helices (Arabic numerals). The helix number 4 in each domain is thought to function as a voltage sensor. The shaker K^+ channel protein (b) isolated from *Drosophila* has only 616 amino acids; it is similar in sequence and transmembrane structure to each of the four domains in the Na^+ channel protein. [From J. Darnell, H. Lodish, and D. Baltimore, *Molecular Cell Biology*, 2nd edn., Scientific American Books, New York, 1990. Adapted from W. A. Catterall, Structure and function of voltage-sensitive ion channels, *Science* **242**:50–61 (1988). Copyright (1988) American Association for the Advancement of Science.]

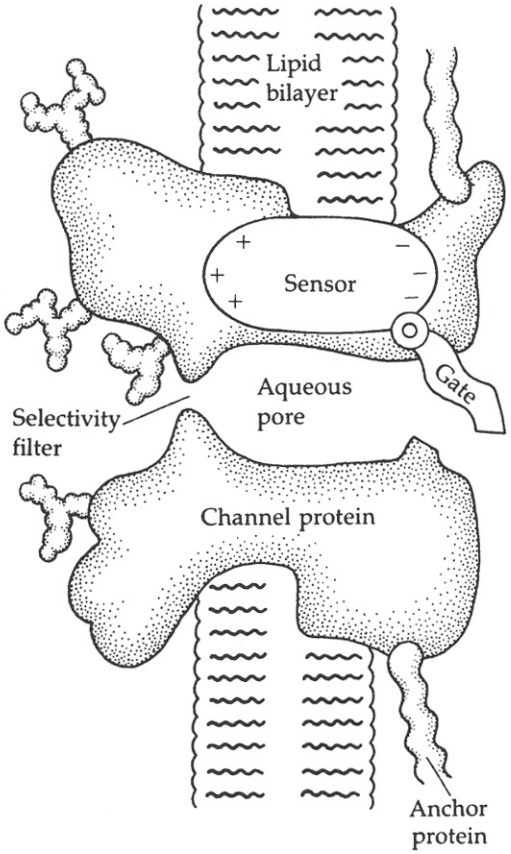

(from Plonsey and Barr)

Figure 4.3. Functional description of membrane channel. "The channel is drawn as a transmembrane macromolecule with a hole through the center. The functional regions—selectivity filter, gate, and sensor—are deduced from voltage clamp experiments and are only beginning to be charted by structural studies. We have yet to learn how they actually look." [From B. Hille, *Ionic Channels of Excitable Membranes*, 2nd edn., Sinauer Associates, Sunderland, MA, 1992.]

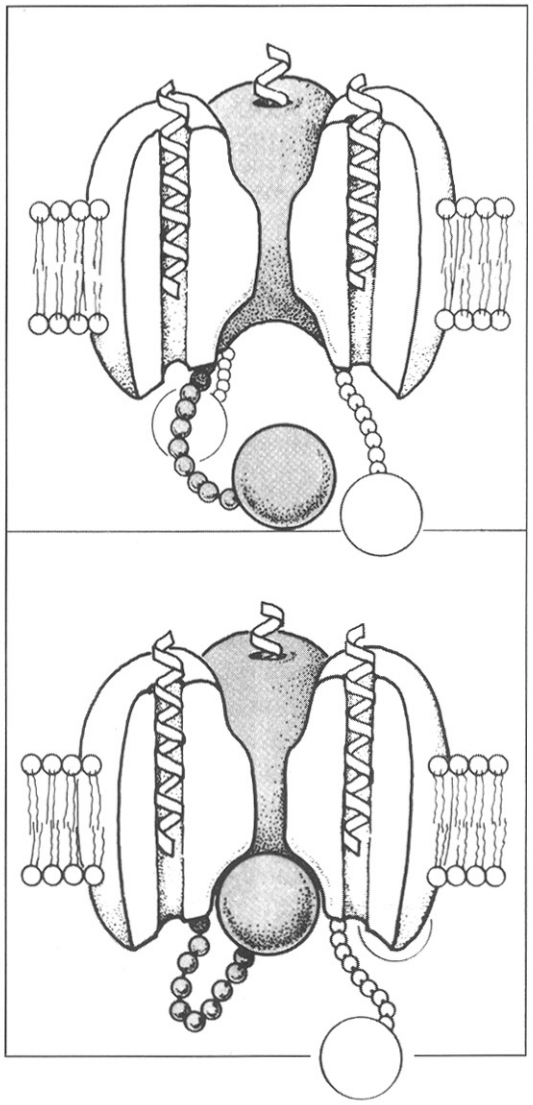

(from Plonsey and Barr)

Figure 4.10. A protein ball pops into a pore formed by the bases of four membrane-spanning proteins (one not shown), thereby stopping the flow of potassium ions out of a nerve cell. Based on Hoshi T, Zagotta WW, Aldrich RW. 1990. Biophysical and molecular mechanisms of *Shaker* potassium channel inactivation. *Science* **250**:506–507, 533–538, 568–571.

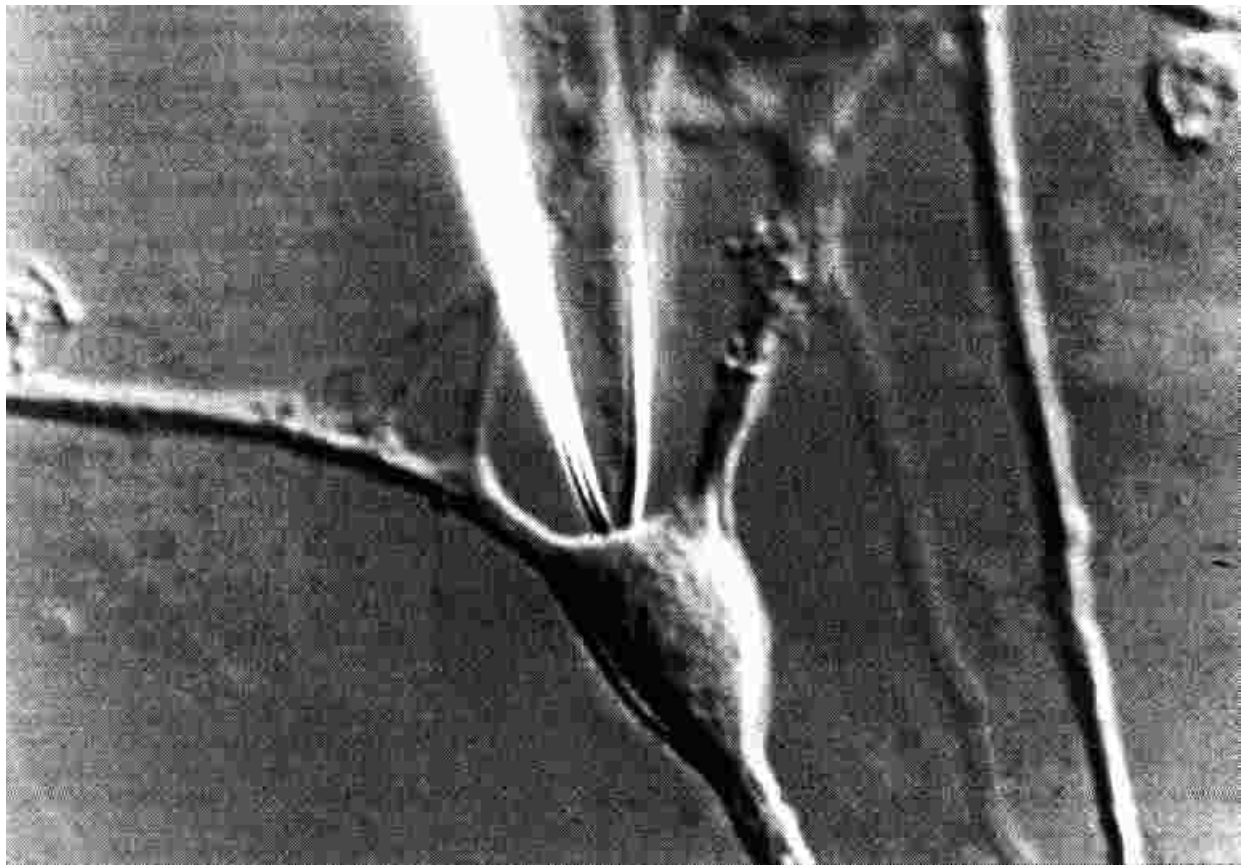

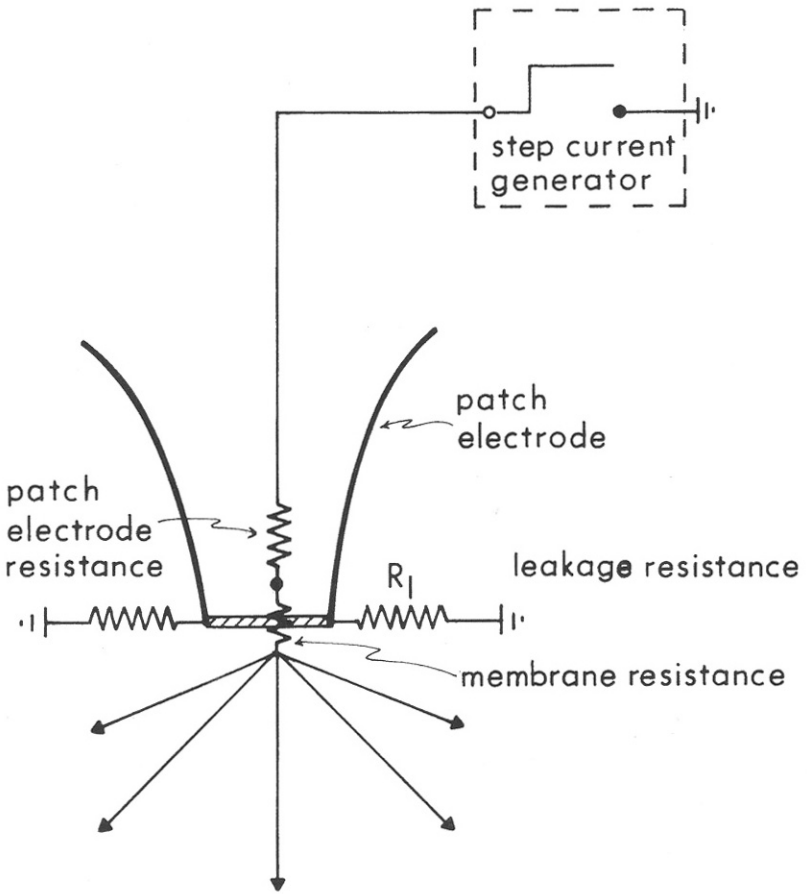

(from Plonsey and Barr)

Figure 4.4. Inside-out patch clamp configuration. The desired current path through the cell is challenged by the alternate (leakage) pathway available in the region of electrode–membrane contact. A single open channel is assumed to give a membrane conductance equal to or greater than 20 pS (a resistance of ≤ 50 GΩ). To keep leakage current low (hence minimal loss of signal strength as well as reduced Johnson noise) this resistance should be in the tens of gigaohms; fortunately, patch electrodes with 100 GΩ leakage resistance are currently available.

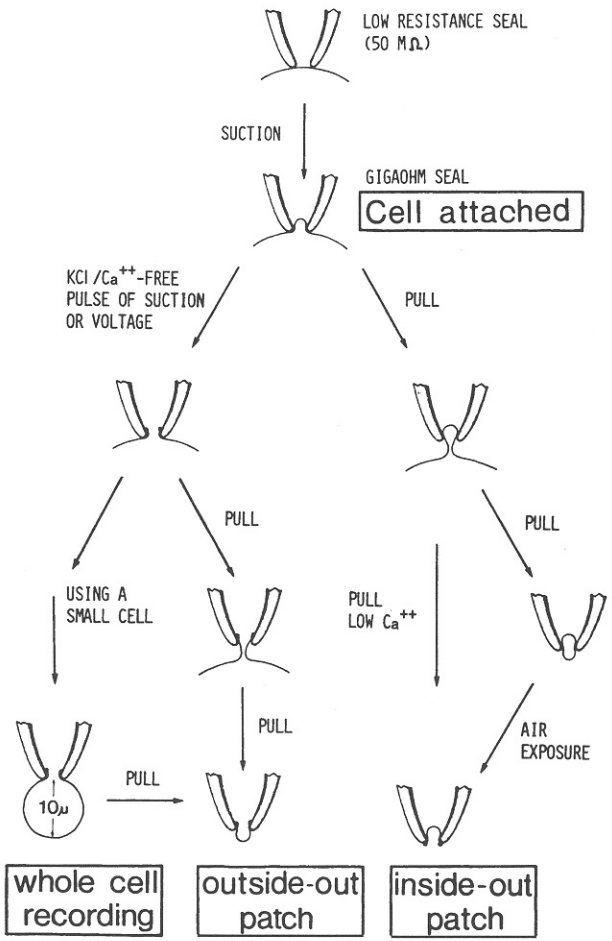

Figure 4.6. Four Configurations for Patch Clamping are described. The clean pipette is pressed against a cell to form a tight seal using light suction, and produces the *cell attached* or *on-cell* configuration. Pulling the pipette away from the cell establishes an *inside–out* patch. Application of a suction pulse disrupts the membrane patch, allowing electrical and diffusional access to the cell interior for *whole-cell* recording. Pulling away from the whole-cell arrangement causes the membrane to re-form into an *outside–out* configuration. From Hamill OP, et al. 1981. Improved patch clamp techniques for high resolution current recording from cells and cell-free membrane patches. *Pflugers Arch* **391**:85–100.

(from Plonsey and Barr)

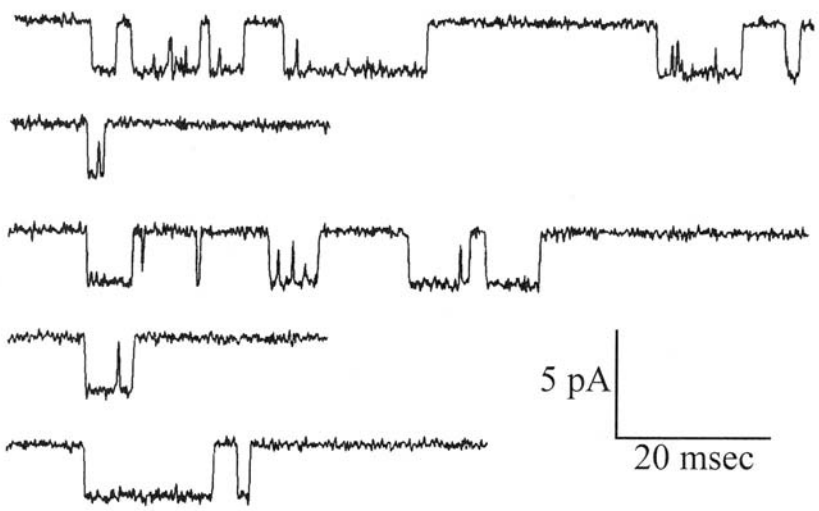

Fig. 8.1 CURRENT FLOWING THROUGH A SINGLE IONIC CHANNEL Several excerpts from a patch-clamp recording of a single acetylcholine-activated channel on a cultured muscle cell. The patch was held at a constant membrane potential of −80 mV. The openings of the channel (downward events) cause a unitary 3-nA current to flow, occasionally interrupted by a brief closing. These closings sometimes fail to reach the baseline due to the limited temporal resolution of the apparatus. Notice the random openings and closings of the channel, characteristic of all ionic channels. Fluctuations in the baseline current are due to thermal noise. Reprinted in modified form by permission from Sigworth (1983).

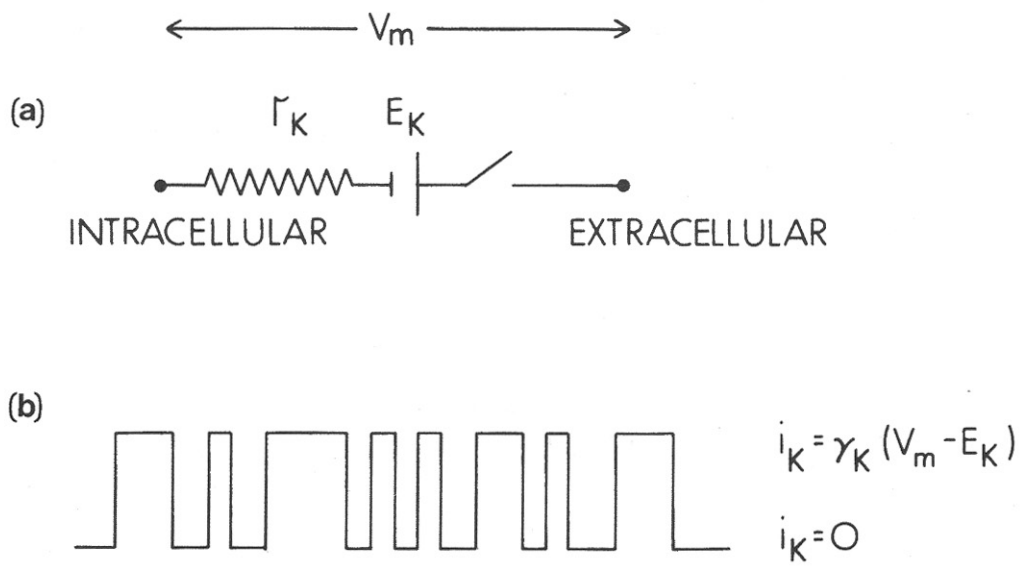

Figure 4.7. (a) Electrical circuit representation for a single (potassium) channel showing fixed resistance r_K, potassium Nernst potential E_K, and the transmembrane potential V_m. The closing and opening of the switch simulates the stochastic opening and closing of the channel gate. (b) Single-channel current corresponding to (a), where $\gamma_K = 1/r_K$. This is an idealization of the recording shown in Fig. 4.6.

(from Plonsey and Barr)

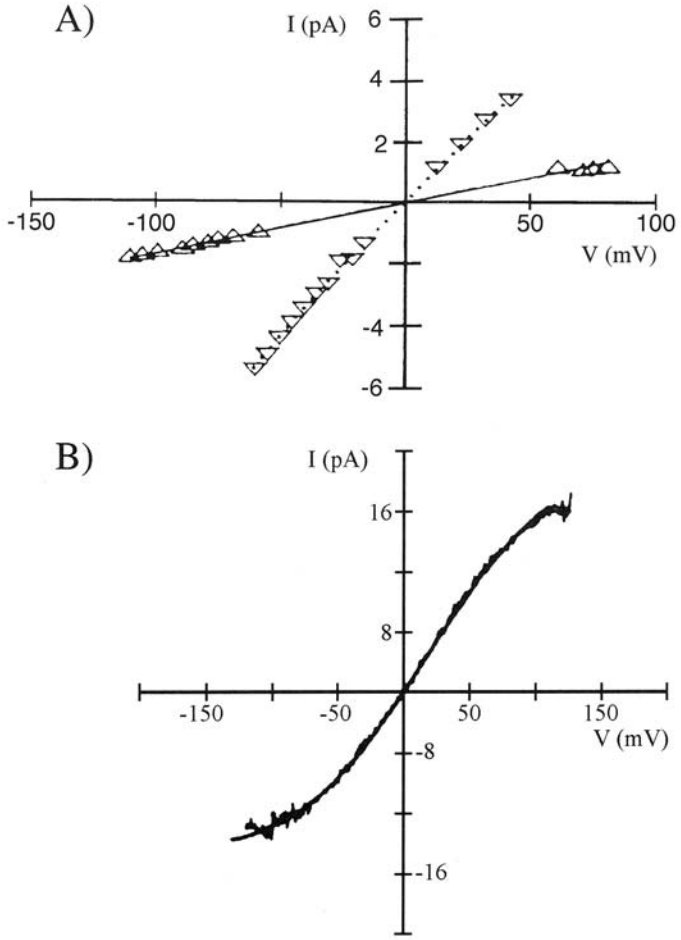

Fig. 8.2 VOLTAGE DEPENDENCY OF IONIC CHANNELS **(A)** Current-voltage relationship of a single nicotinic ACh-activated ionic channel. Since the concentration of the permeant ion on both sides of the membrane is identical (here set to either 150 m*M* NH_4^+ (downward pointing arrowhead) or Li^+ (upward pointing arrowhead)), the reversal potential is zero. As the voltage gradient across the channel increases, so does the current through the channel (up to a limit), in accordance with Ohm's law. The single-channel conductance γ is either 17 pS (in Li^+) or 79 pS (in NH_4^+). Reprinted in modified form by permission from Dani (1989). **(B)** I–V relationship for a single voltage- and calcium-dependent potassium channel in a symmetrical 160-mM potassium solution. The slope of this curve around the origin is 265 pS. Deviations from Ohm's law are apparent for large voltage gradients. Reprinted in modified form by permission from Yellen (1984).

TABLE 8.1
Properties of Different Types of Ionic Channels

Channel type	Preparation	γ	η
Fast Na^+	Squid giant axon[1]	14	330
Fast Na^+	Rat axonal node of Ranvier[2]	14.5	700
Fast Na^+	Pyramidal cell body[3]	14.5	4–5
Delayed rectifier K^+	Squid giant axon[4]	20	18
Ca^{2+}-dependent K^+	Mammalian preparation[5]	130–240	—
Transient A current	Insect, snail, mammal[5]	5–23	—
Nicotinic ACh receptor	Mammalian motor endplate[7]	20–40	10,000
$GABA_A$ Cl^- receptor	Hippocampal granule cells[8]	14, 23	—

Single channel conductance γ (in pS) and average channel density η if known (per μm^2) for some ionic channels. The exact value of γ depends on many variables, in particular the temperature and the composition of the extracellular fluid.

[1] In the absence of external divalent ions at 5° C; Bezanilla (1987).

[2] At 20° C; Neumcke and Stämpfli (1982).

[3] Hippocampal pyramidal cell body and initial segment at 24° C; Colbert and Johnston (1996).

[4] Between 13–25° C; less frequent are channels with $\gamma = 10$ and 40 nS; Llano, Webb, and Bezanilla (1988).

[5] At 22° C; Latorre and Miller (1983).

[6] At 22° C; Adams and Nonner (1989).

[7] Peak density; the density decreases with distance from active zone; for a review, see Hille (1992).

[8] At 22° C; Edwards, Konnerth, and Sakmann (1990).

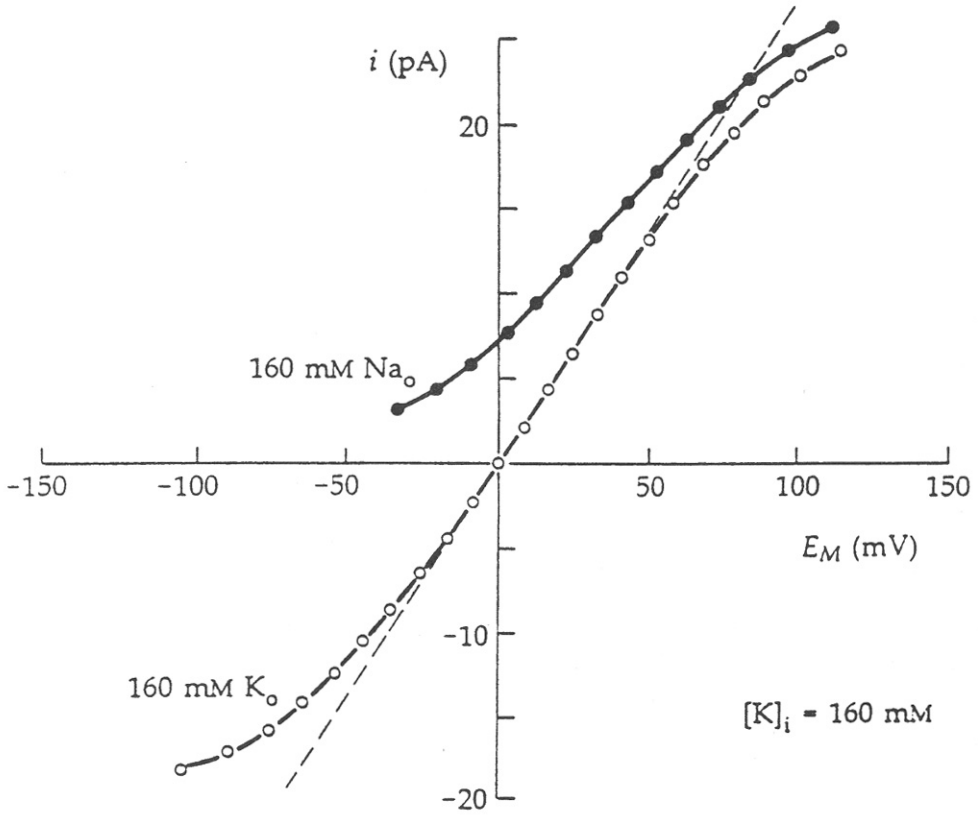

Figure 4.8. Current–voltage relations for a single BK K(Ca) channel of bovine chromaffin cell. The excised outside-out patch was bathed in 160 mM KCl or NaCl and the patch pipette contained 160 m M KCl. In symmetrical K solutions the slope of the dashed line is $\gamma = 265$ pS. $T = 23$ °C. [From B. Hille, *Ionic Channels of Excitable Membranes*, 2nd edn., Sinauer Associates, Sunderland, MA, 1992; based on measurements of G. Yellen, Ionic permeation and blockade in a Ca^{2+}-activated K^+ channels of bovine chromaffin cells, *J. Gen. Physiol.* **84**:157–186 (1984).]

(from Plonsey and Barr)

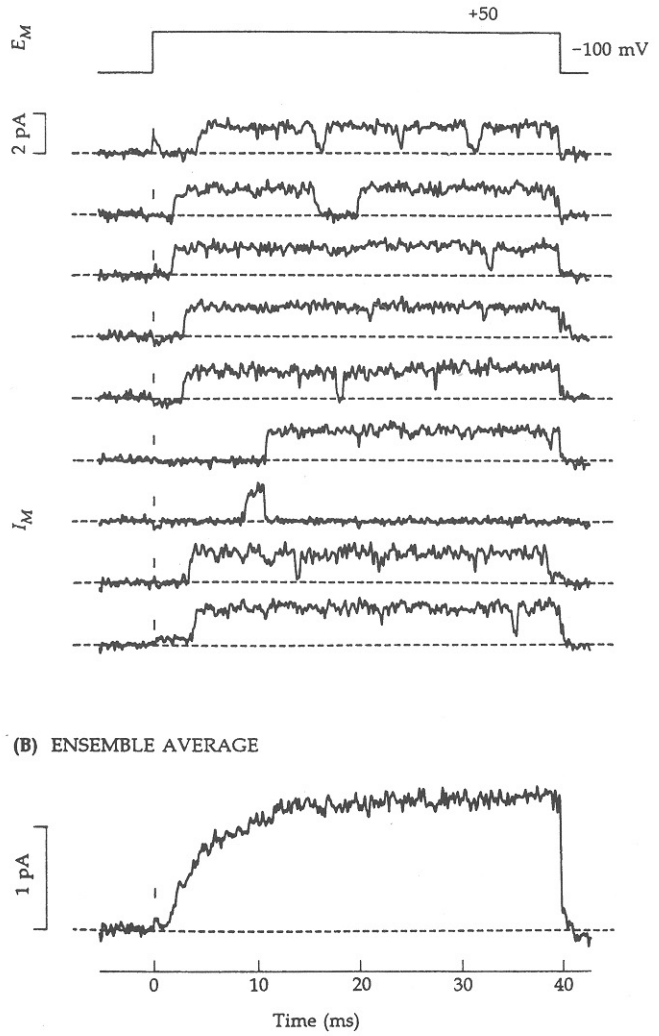

Figure 4.6. Patch clamp recording of unitary K currents in a squid giant axon during voltage steps from −100 to 50 mV. To avoid the overlying Schwann cells the axon was cut open and the patch electrode sealed against the *cytoplasmic* face of the membrane. (A) Nine consecutive trials showing channels of 20 pS conductance filtered at 2 kHz bandwidth. (B) Ensemble mean of 40 repeats; these reveal the expected macroscopic behavior. $T = 20$ °C. [From F. Bezanilla and G. R. Augustine in B. Hille, *Ionic Channels of Excitable Membranes*, 2nd edn., Sinauer Associates, Sunderland, MA, 1992.]

(from Plonsey and Barr)

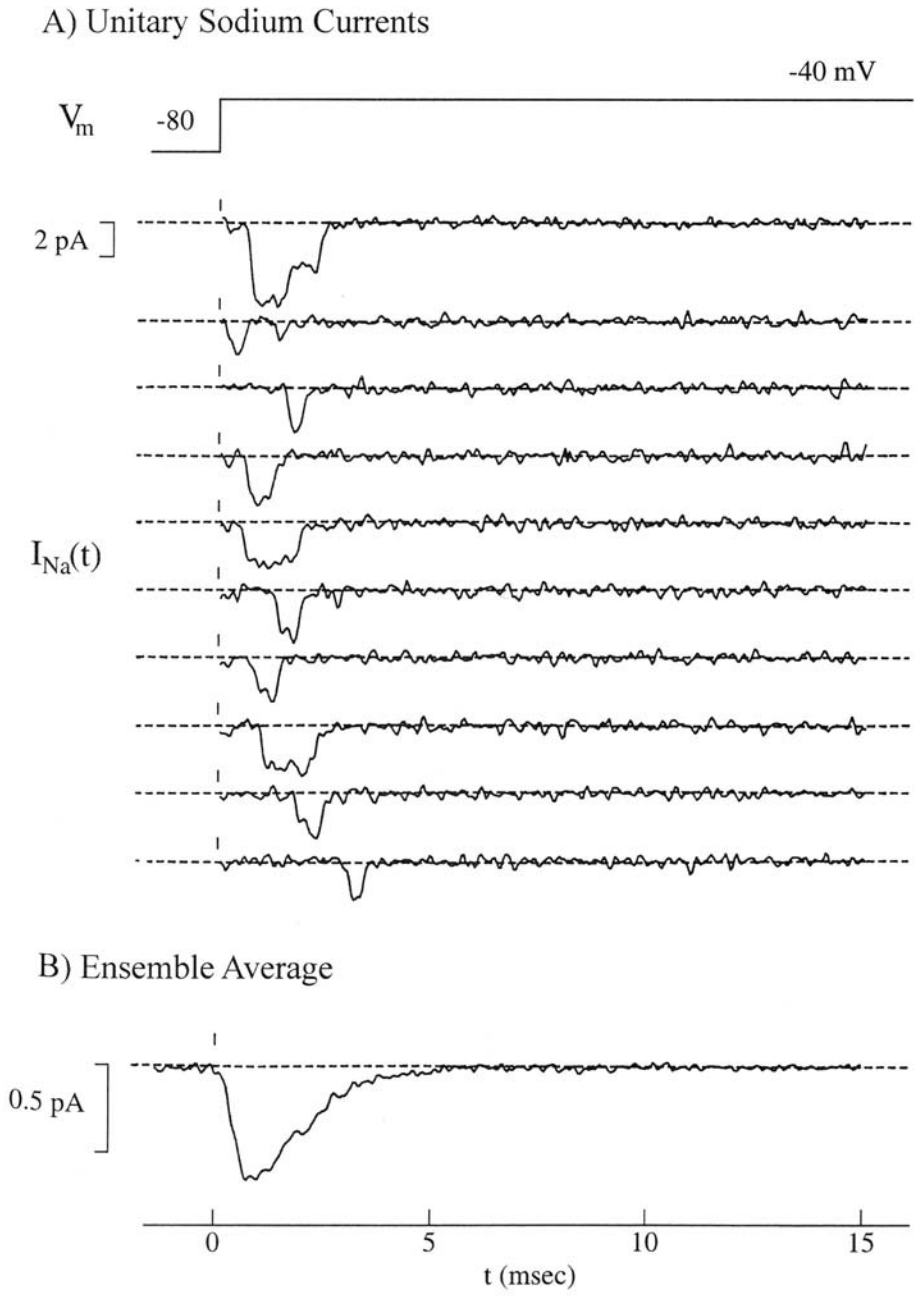

Fig. 8.6 Stochastic Openings of Individual Sodium Channels (A) Random opening and closing of a handful of fast sodium channels in a mouse muscle cell. The membrane potential was stepped from −80 to −40 mV; the first trial reveals the simultaneous opening of two Na^+ channels, while on all other trials, only a single channel was open. **(B)** Averaging over 352 such trials leads to a smoothly varying current in accordance with the m^3h model of Hodgkin and Huxley. Experiment carried out at 15° C. Reprinted by permission from Patlak and Ortiz (1986).

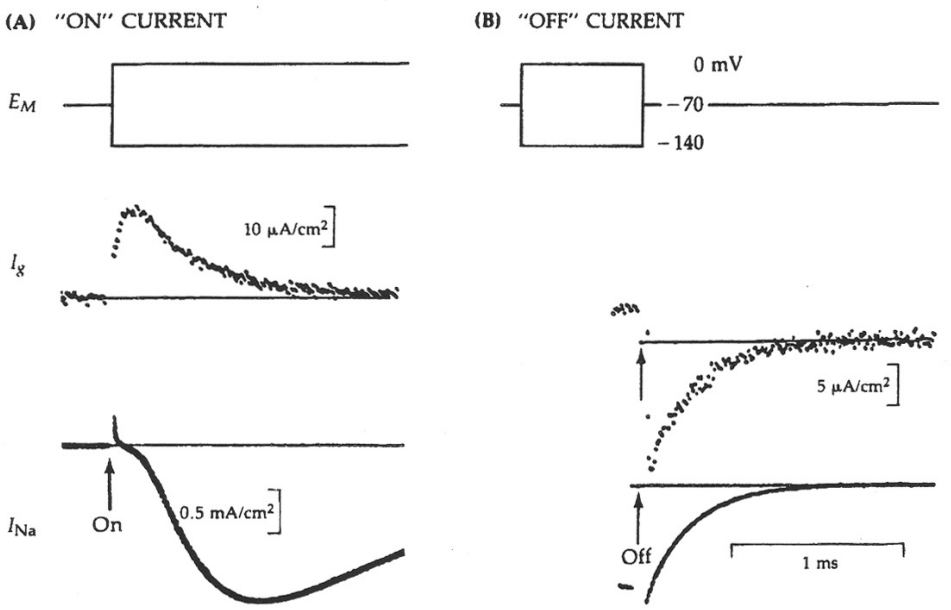

(from Johnston and Wu)

Figure 6.22 Gating current (I_g) and I_{Na} recorded by adding responses to symmetrical positive and negative pulses applied to the squid giant axon. I_g was measured in Na^+-free solutions with TTX to block Na^+ channels and internal Cs^+ to block K^+ channels. Since I_g is small, 50 traces had to be averaged in the recording computer to reduce the noise. I_{Na} is measured in normal artificial sea water without TTX. (A) Depolarization from rest elicits an outward "on" I_g that precedes opening of Na^+ channels. (B) Repolarization elicits an inward "off" I_g coinciding with closing of channels (a different axon). (From Hille 1992, adapted from Armstrong and Bezanilla 1974 by copyright permission of the Rockefeller University Press.)

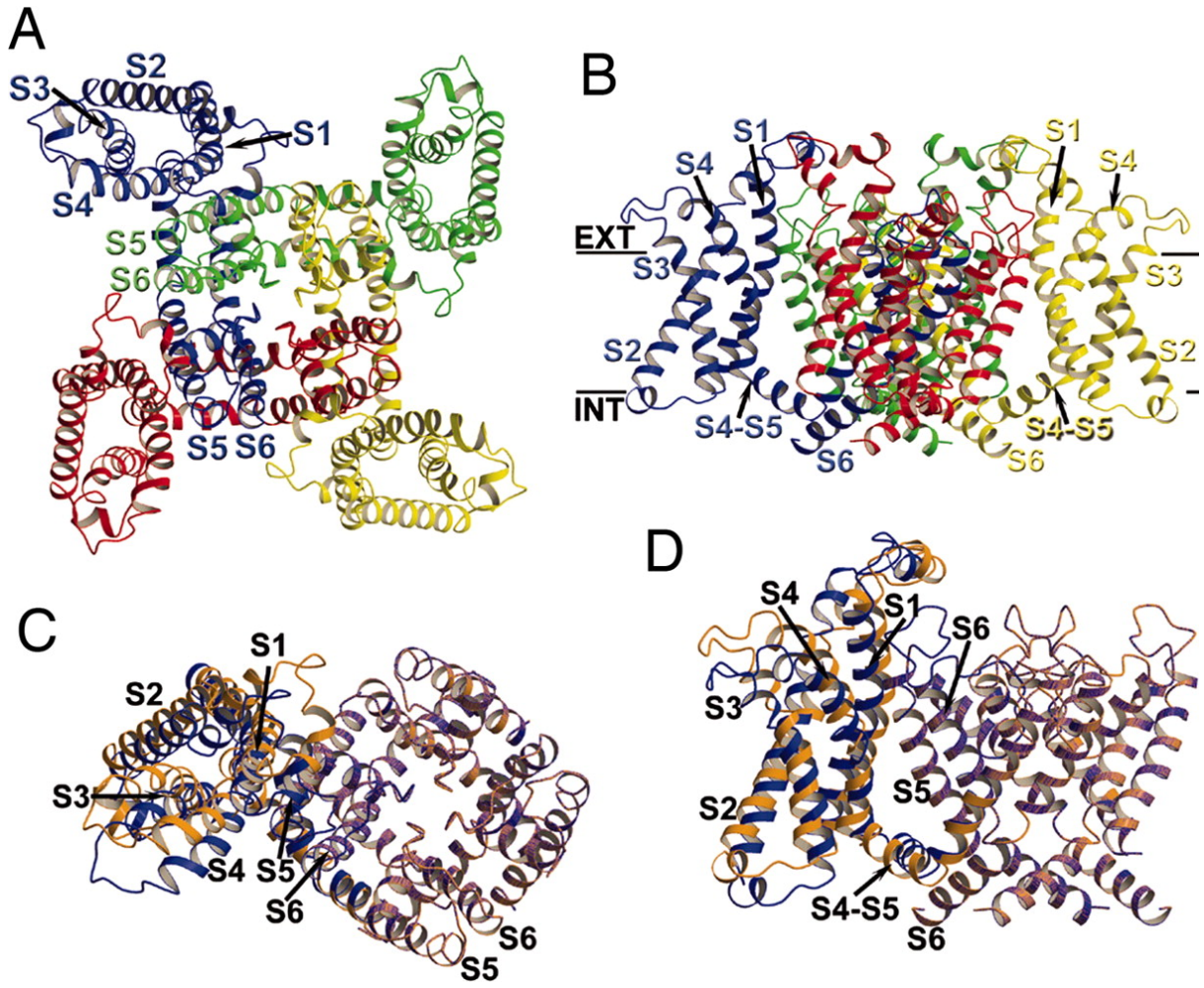

(Yarov-Yarovoy *et al.*, PNAS 2006)

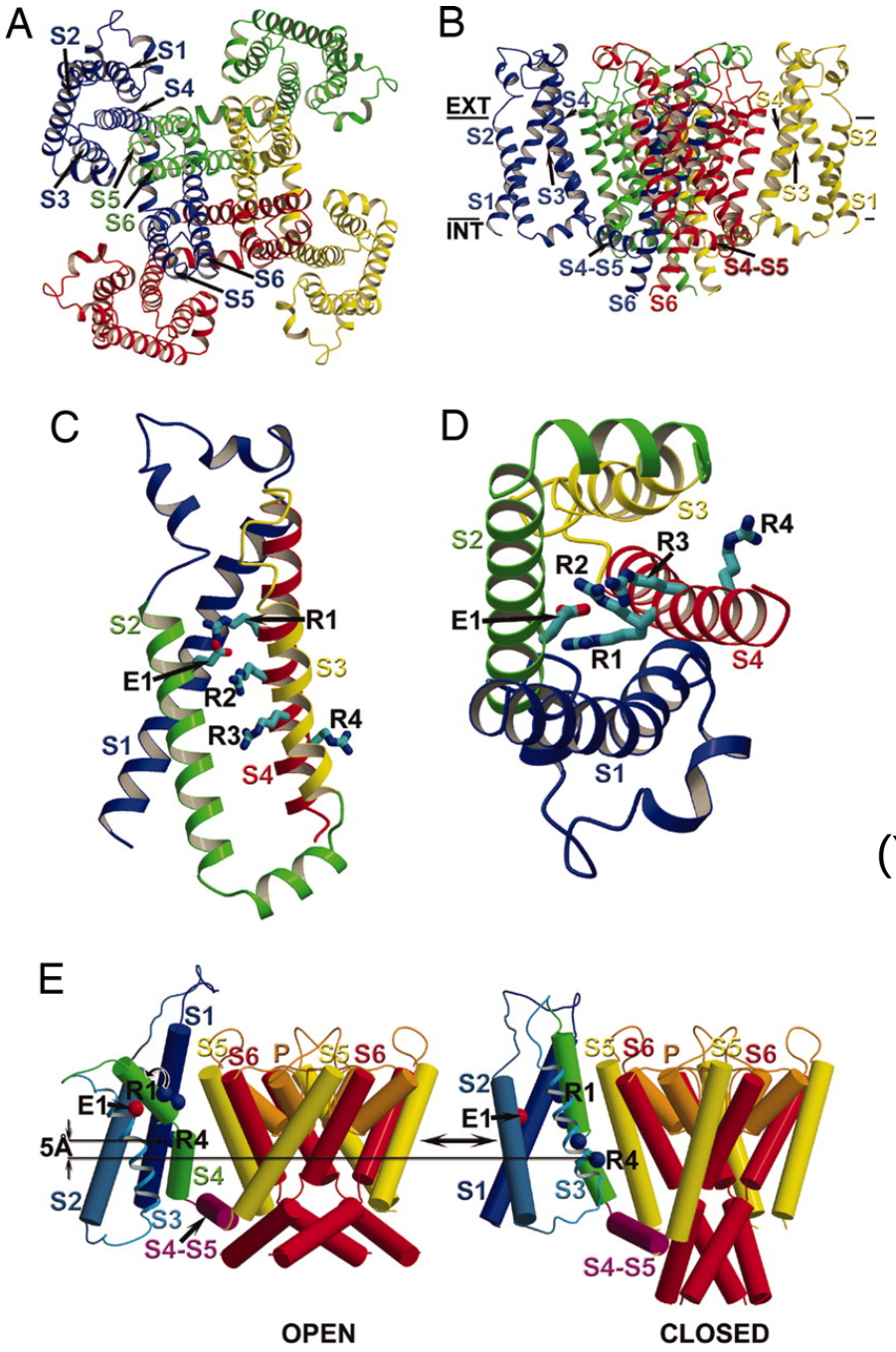

(Yarov-Yarovoy *et al.*, PNAS 2006)

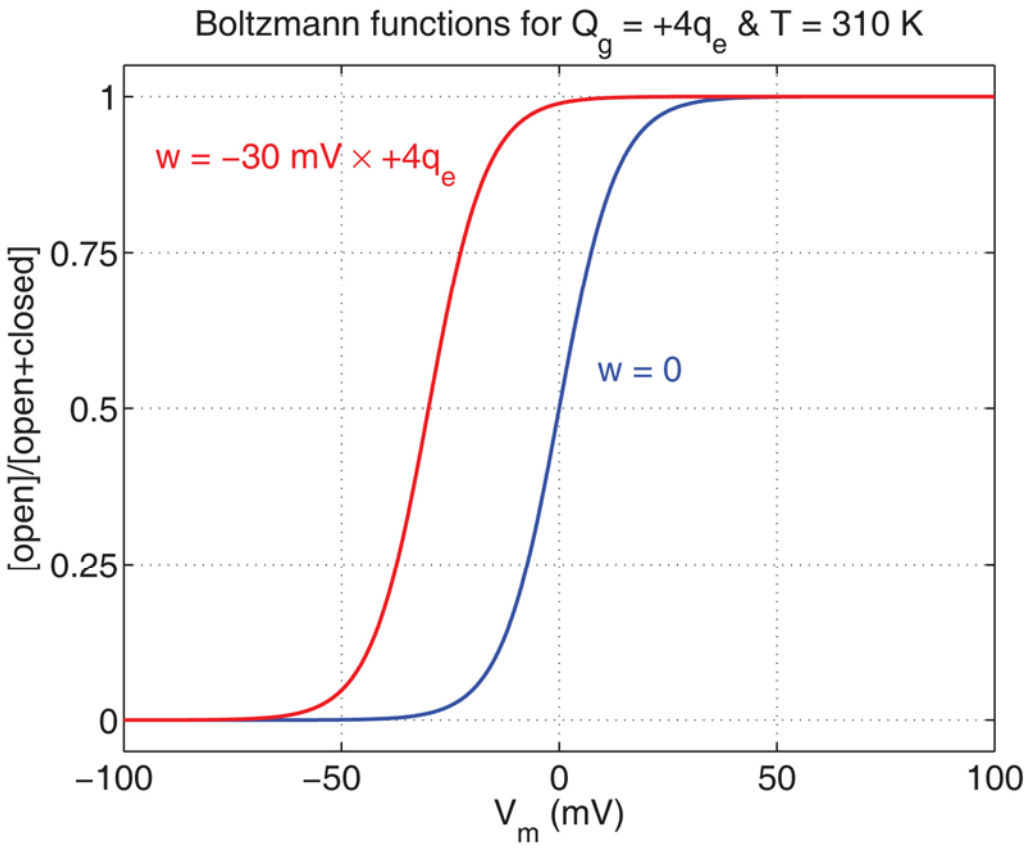
Boltzmann functions for $Q_g = +4q_e$ & T = 310 K
w = −30 mV × $+4q_e$
w = 0
[open]/[open+closed]
1
0.75
0.5
0.25
0
−100
−50
0
50
100
V_m (mV)

Kinetic model of sodium channel

$$
\begin{array}{ccccccc}
m_0h_0 & \underset{\beta_m}{\overset{3\alpha_m}{\rightleftharpoons}} & m_1h_0 & \underset{2\beta_m}{\overset{2\alpha_m}{\rightleftharpoons}} & m_2h_0 & \underset{3\beta_m}{\overset{\alpha_m}{\rightleftharpoons}} & m_3h_0 \\
\alpha_h \Big\Downarrow \beta_h & & \alpha_h \Big\Downarrow \beta_h & & \alpha_h \Big\Downarrow \beta_h & & \alpha_h \Big\Downarrow \beta_h \\
m_0h_1 & \underset{\beta_m}{\overset{3\alpha_m}{\rightleftharpoons}} & m_1h_1 & \underset{2\beta_m}{\overset{2\alpha_m}{\rightleftharpoons}} & m_2h_1 & \underset{3\beta_m}{\overset{\alpha_m}{\rightleftharpoons}} & m_3h_1
\end{array}
$$

The number of channels in the state m_3h_1 determines the sodium conductance.

Kinetic model of potassium channel

$$n_0 \underset{\beta_n}{\overset{4\alpha_n}{\rightleftharpoons}} n_1 \underset{2\beta_n}{\overset{3\alpha_n}{\rightleftharpoons}} n_2 \underset{3\beta_n}{\overset{2\alpha_n}{\rightleftharpoons}} n_3 \underset{4\beta_n}{\overset{\alpha_n}{\rightleftharpoons}} n_4$$

The number of channels in the state n_4 determines the potassium conductance.

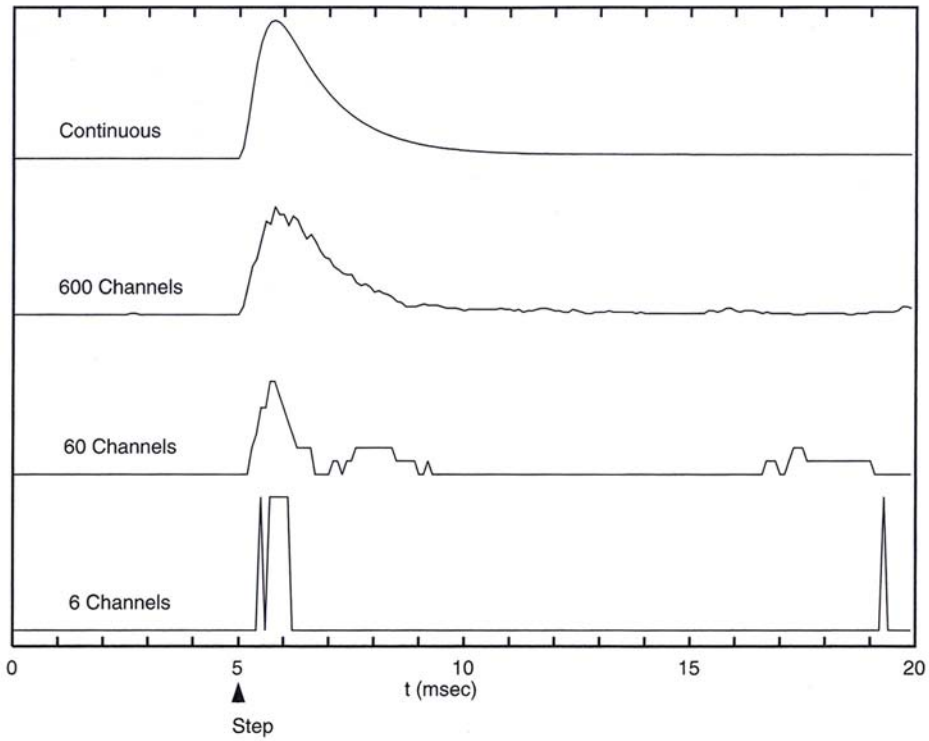

Fig. 8.7 Simulated Life History of Individual Sodium Channels The membrane potential in a simulated membrane patch containing a variable number of Na^+ channels was stepped from $V_0 = 0$ to $V_1 = 50$ mV at 5 msec (arrow). The normalized conductance associated with the eight-state Markov model shown in Fig. 8.5 was evaluated numerically for several trial runs (see Strassberg and DeFelice, 1993). As the number of channels is increased from 6 to 600, the graded and deterministic nature of the (normalized) sodium conductance emerges from the binary and stochastic single-channel behavior. The top trace shows the conductance computed using the continuous time-course (approximating $(1 - e^{-t/\tau_m})^3 e^{-t/\tau_h}$) formalism of Hodgkin and Huxley (1952). This figure should be compared against the experimentally recorded sodium current through a few channels in Fig. 8.6B. Reprinted in modified form by permission from Strassberg and DeFelice (1993).

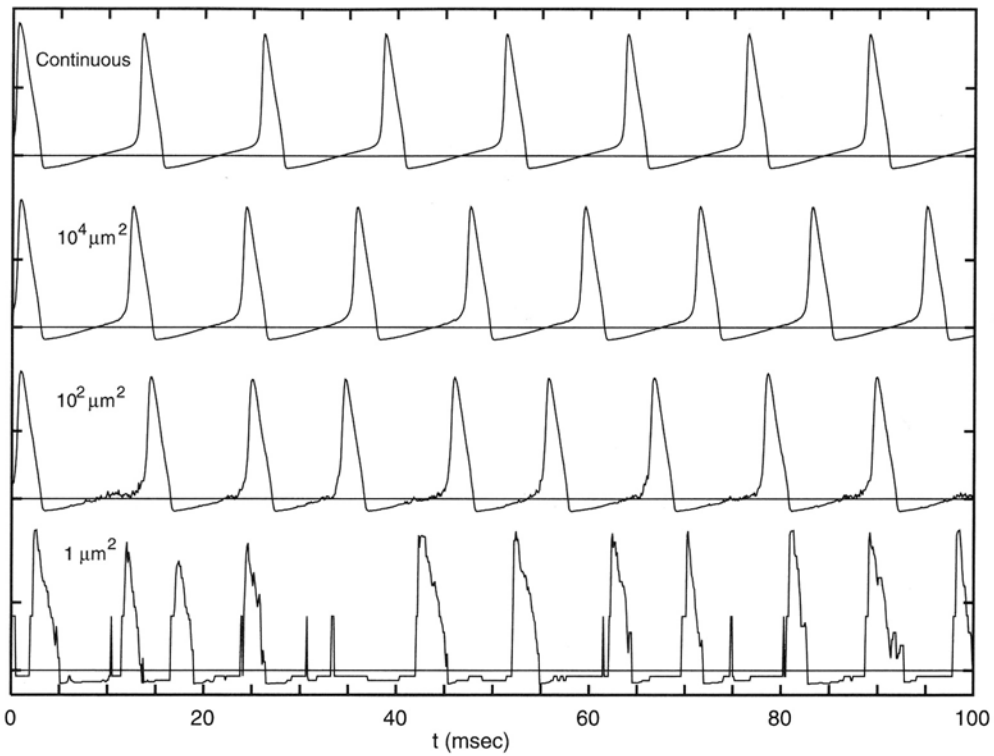

Fig. 8.8 Action Potentials and Single Channels Computed membrane potential (relative to V_{rest} indicated by horizontal lines) in different size patches of squid axon membrane populated by a constant density of Na^+ and K^+ channels. The space-clamped membrane is responding to a current injection of 100 pA/μm^2. The transitions of each all-or-none channel are described by its own probabilistic Markov model (the eight-state model in Fig. 8.5 for the Na^+ channel and the simplest possible five-state linear model for the K^+ channel). For patches containing less than 100 channels (bottom trace), firing can be quite irregular. For patches containing dozens or fewer channels it becomes impossible to define action potentials unambiguously, since the opening of one or two channels can rapidly depolarize the membrane (not shown). As the membrane potential acts on 1000 or more binary and stochastic channels, the response becomes quite predictable, and merges into the behavior expected by numerical integration of the Hodgkin–Huxley equations for continuous and deterministic currents (top trace). The density is set to 60 Na^+ channels and 18 K^+ channels per square micrometer, each with a single channel conductance γ of 20 pS. All other values are as specified in the standard Hodgkin–Huxley model. Reprinted in modified form by permission from Strassberg and DeFelice (1993).

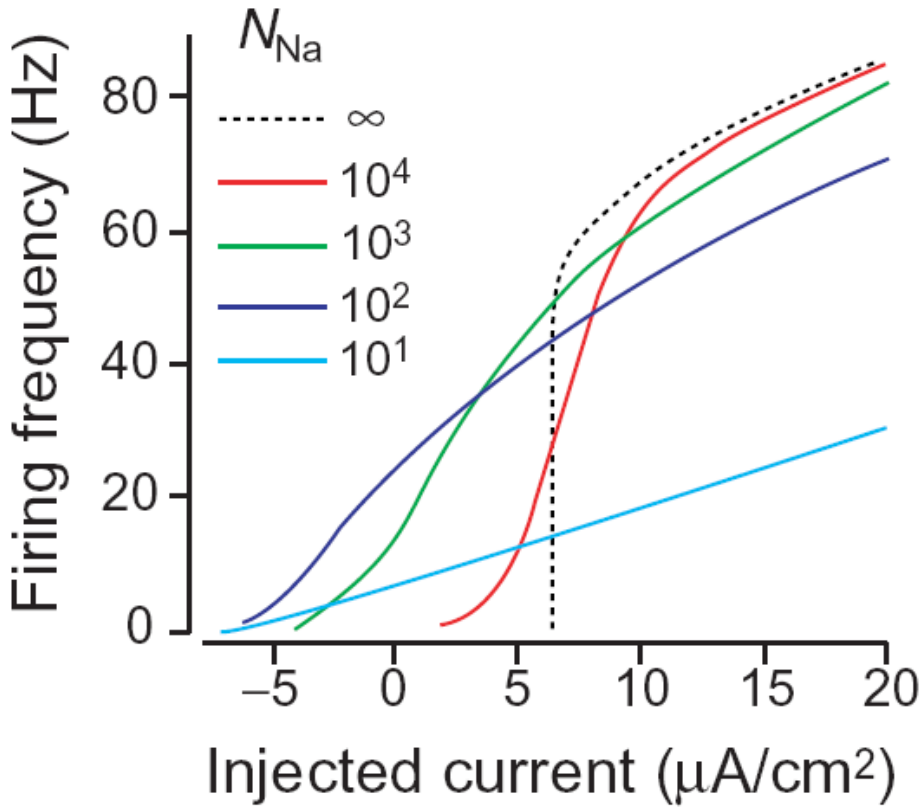

(from White et al.,
Trends Neurosci., 2000)

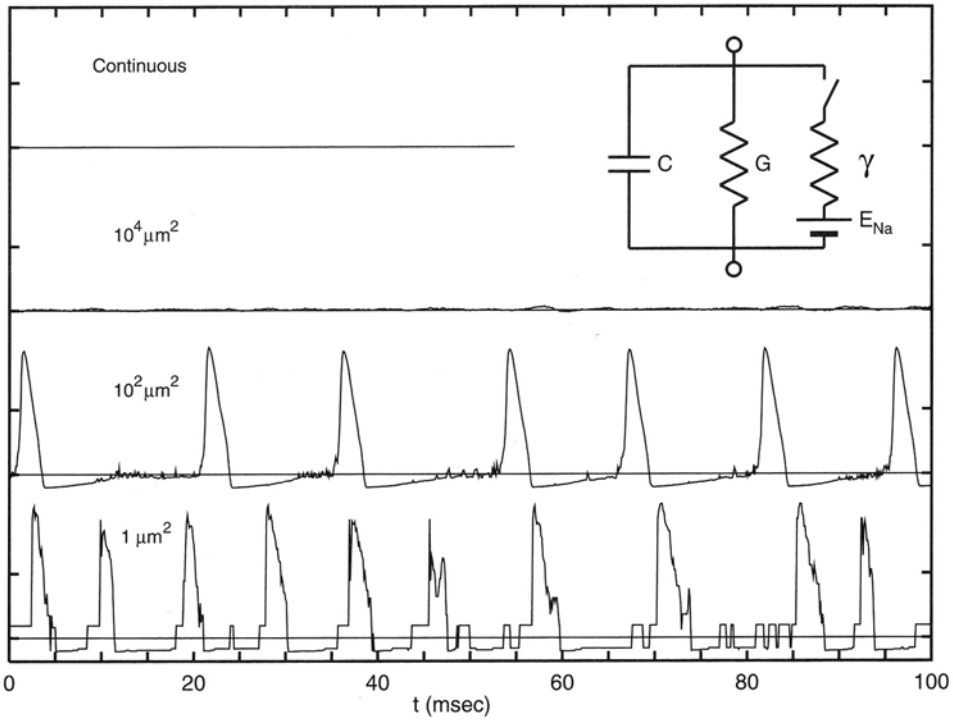

Fig. 8.9 Spontaneous Action Potentials The same model as is Fig. 8.8 is rerun, but now in the absence of *any* current stimulus. The bottom three traces show Monte-Carlo sample trials for axonal membrane patches of different surface areas A populated with a constant density of Na^+ and K^+ channels (60 and 18 channels per square micrometer, respectively). Because the opening of a single sodium channel (of conductance γ) can give rise to a very large depolarization, the spontaneous openings of two sodium channels is enough to trigger the opening of the remaining sodium channels and the membrane generates a spike. These spikes are Poisson distributed (once a refractory period has been accounted for; Chow and White, 1996). The top trace shows the solution of the continuous and deterministic Hodgkin–Huxley equation: V in the absence of a current input remains flat. The circuit inset provides the basic intuition why a single channel, in the presence of a small leak conductance G, can cause a large membrane depolarization. These simulations predict that in high-impedance systems with an active membrane, spontaneous spiking can be observed under certain conditions in the absence of any synaptic input. The membrane leak conductance G for these three conditions corresponds to 3 pS, 300 pS, and 30 nS, as compared to a single-channel conductance of $\gamma = 20$ pS for both channel types. For more details see legend to Fig. 8.8. Reprinted in modified form by permission from Strassberg and DeFelice (1993).

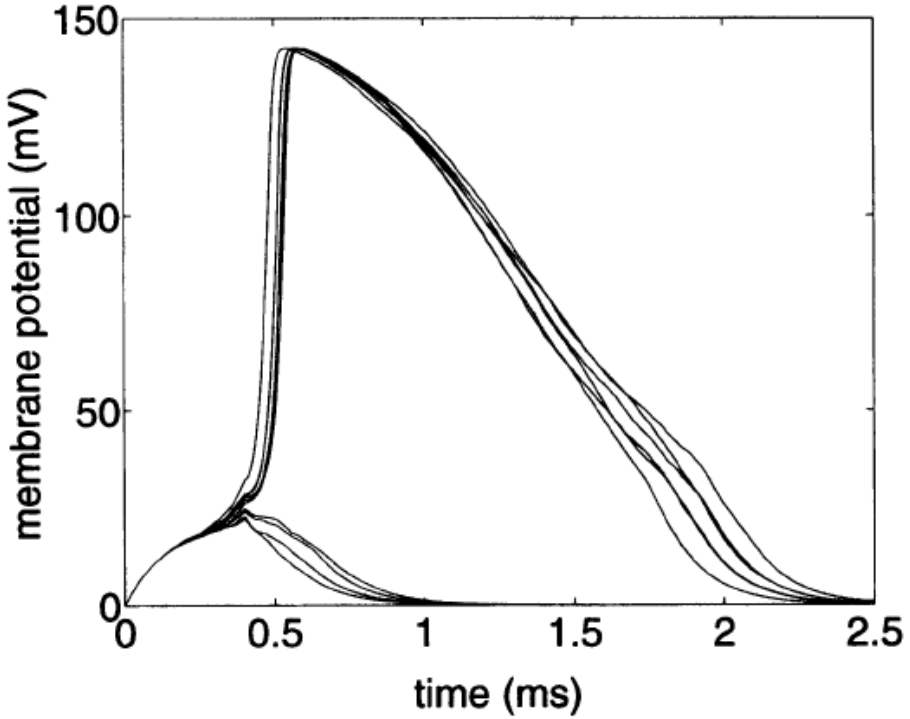

FIGURE 2 Membrane potential response produced by stochastic model to 10 identical near-threshold stimuli. There are 4000 voltage-sensitive sodium channels. Stimuli are 400 μs monophasic rectangular current pulses. Membrane potential is shifted relative to the resting potential.

(from Rubinstein,
Biophys. J., 1995)

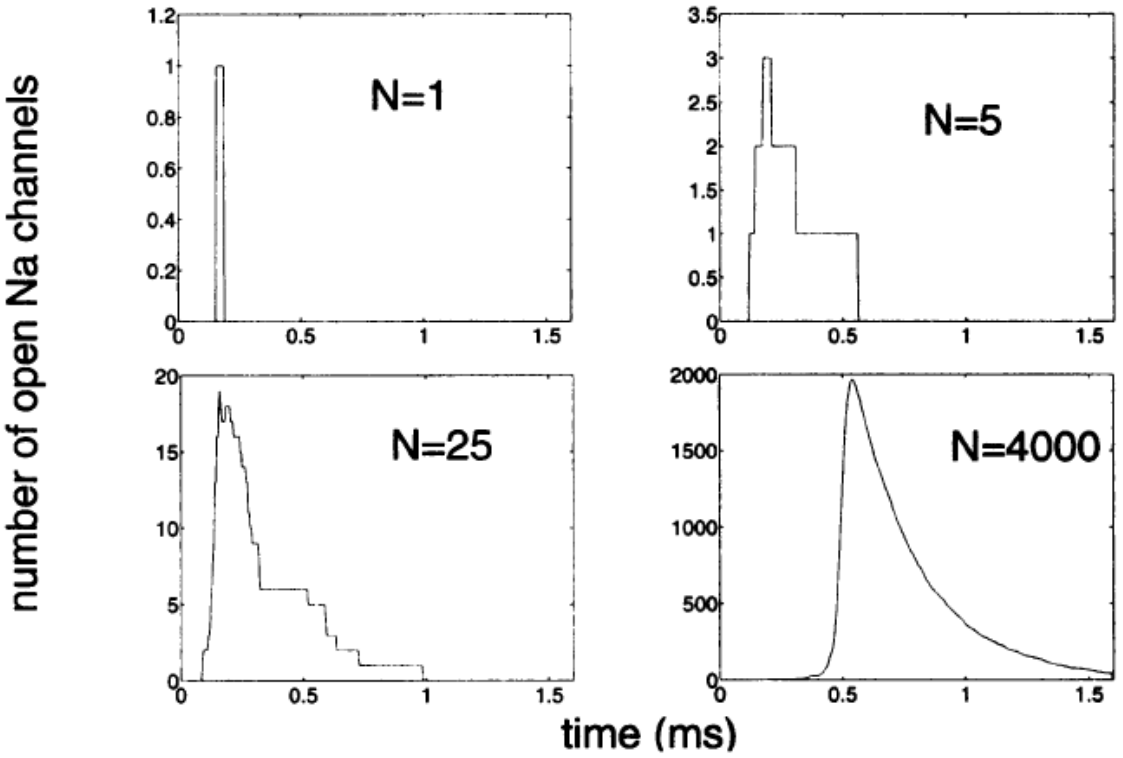

FIGURE 3 Number of open sodium channels during action potential for four different values of N, the total number of voltage-sensitive sodium channels. With increasing N the passive membrane conductance and capacitance are increased proportionately, effectively increasing the nodal surface area. Stimuli are near-threshold, but somewhat greater current densities are required for smaller values of N, resulting in shorter latencies.

(from Rubinstein,
Biophys. J., 1995)

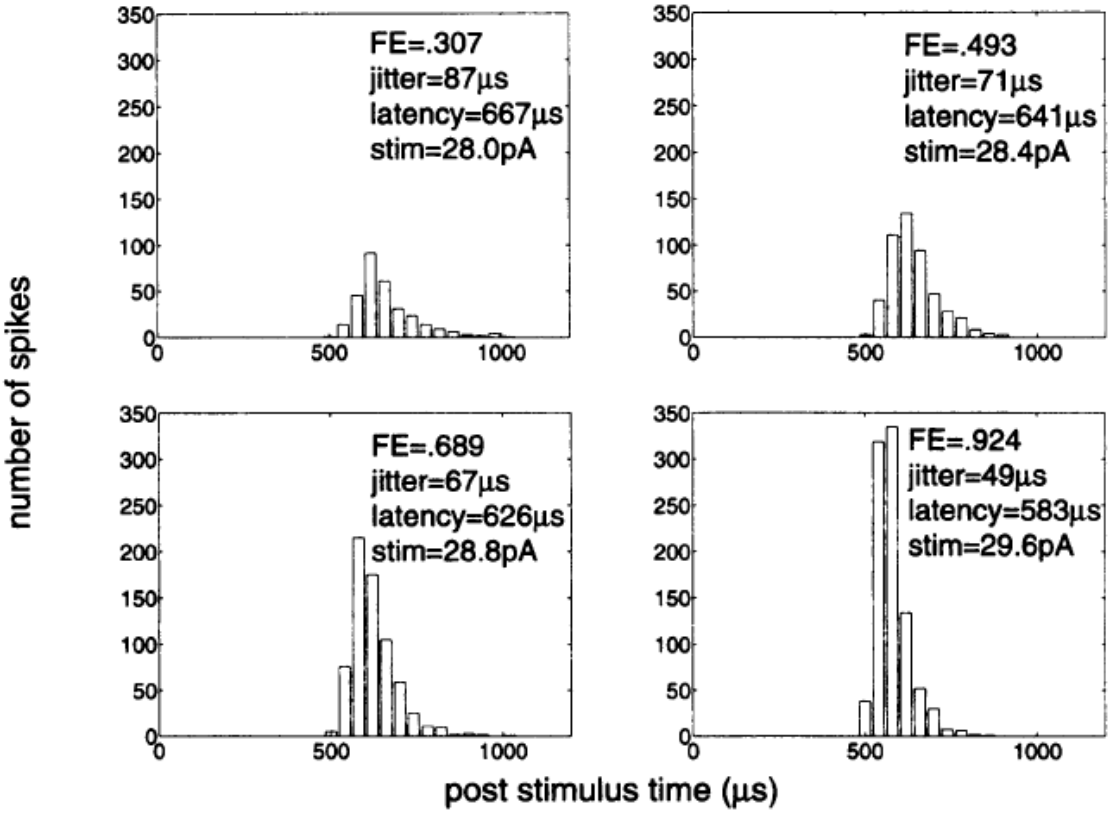

FIGURE 4 PST Histograms at four different stimulus intensities. $N = 4000$. Firing efficiency (FE) is number of spikes divided by number of stimuli (1000). Latency and jitter are given by the histogram's mean and standard deviation, respectively. Spike time is defined when the membrane potential crosses 75 mV relative to rest, on the upstroke of the action potential.

(from Rubinstein,
Biophys. J., 1995)

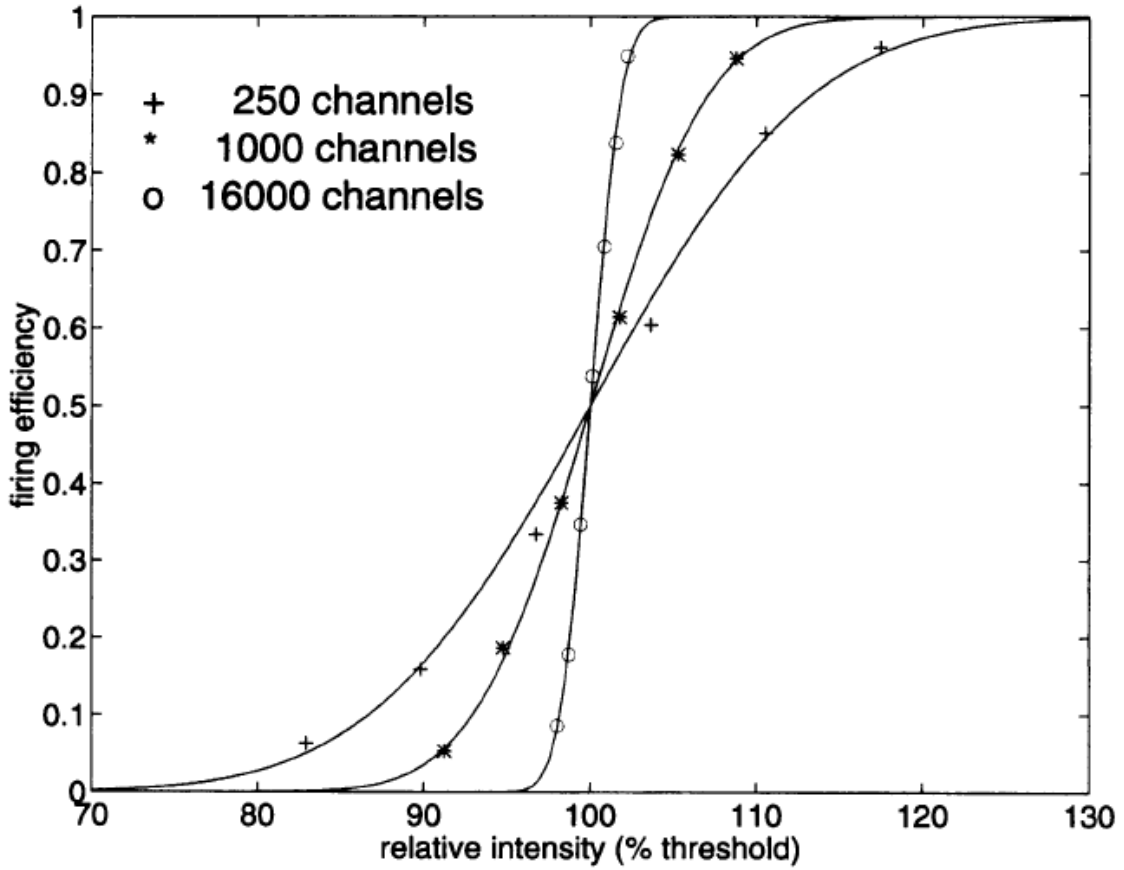

FIGURE 5 Input-Output functions for $N = 250$, 1,000, and 16,000. With increasing N, there is a steeper slope and a smaller relative spread of threshold (RS).

(from Rubinstein,
Biophys. J., 1995)

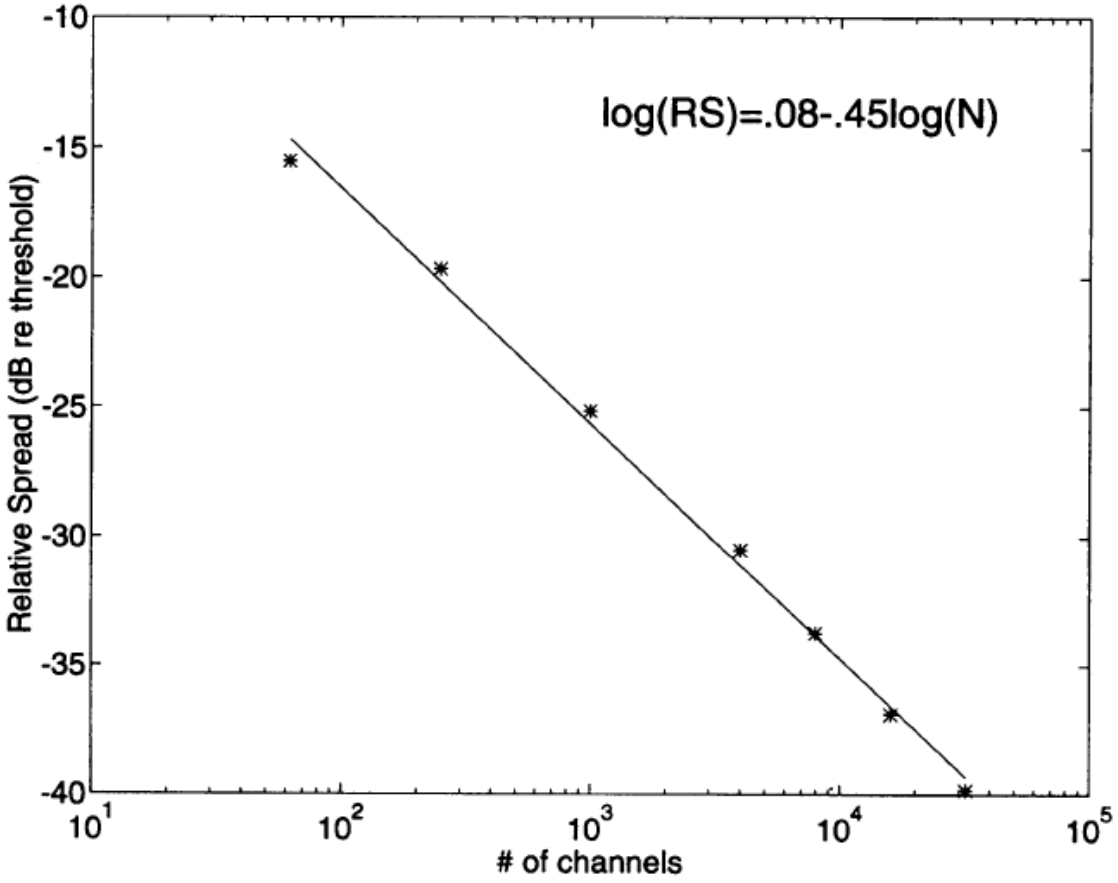

FIGURE 6 Relationship between number of channels, N, and the RS. The equation is a linear fit to the logarithmically transformed data. The slope of -0.45 is consistant with a binomial process whose standard deviation is proportional to $N^{-1/2}$.

(from Rubinstein,
Biophys. J., 1995)

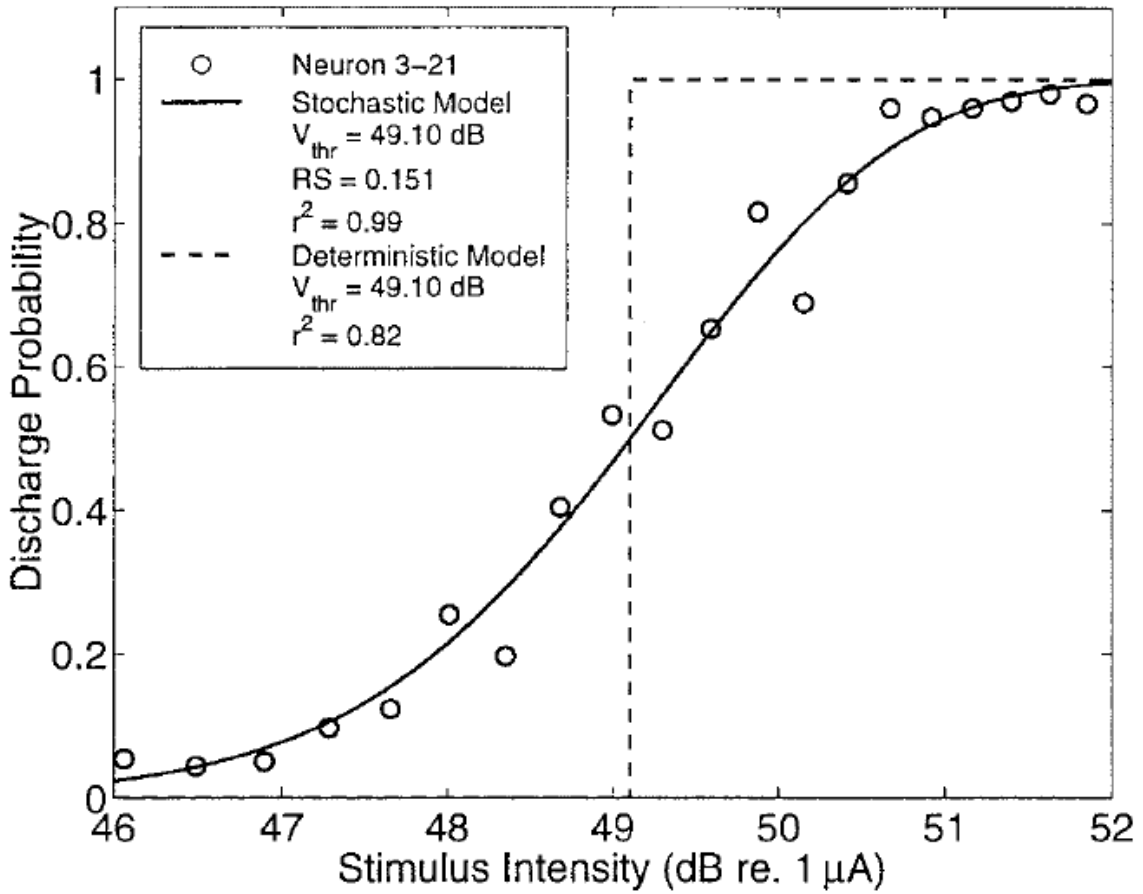

Fig. 3. Stochastic (solid line) and deterministic (dashed line) model fits to discharge probability data (o) [38, Neuron 3-21] for a single biphasic pulse of duration 100 μs/phase.

(from Bruce et al.,
IEEE TBME, 1999a)

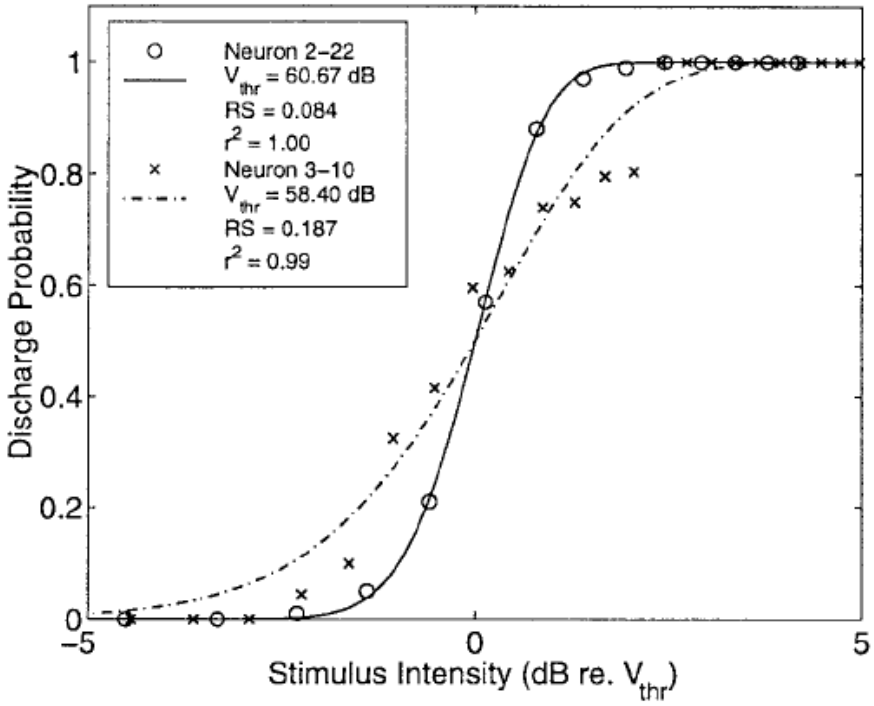

(a)

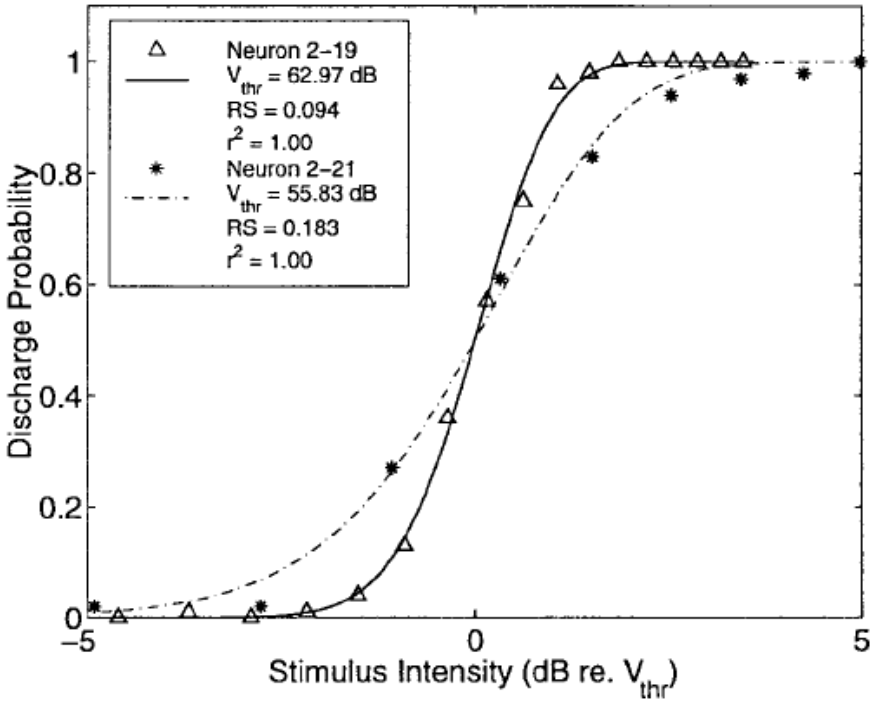

(b)

Fig. 4. Fits to fiber I/O functions from [38] for a single pulse. (a) 200 us/phase and (b) 400 us/phase. Note that the abscissa is stimulus intensity relative to the fiber's threshold.

(from Bruce et al.,
IEEE TBME, 1999a)

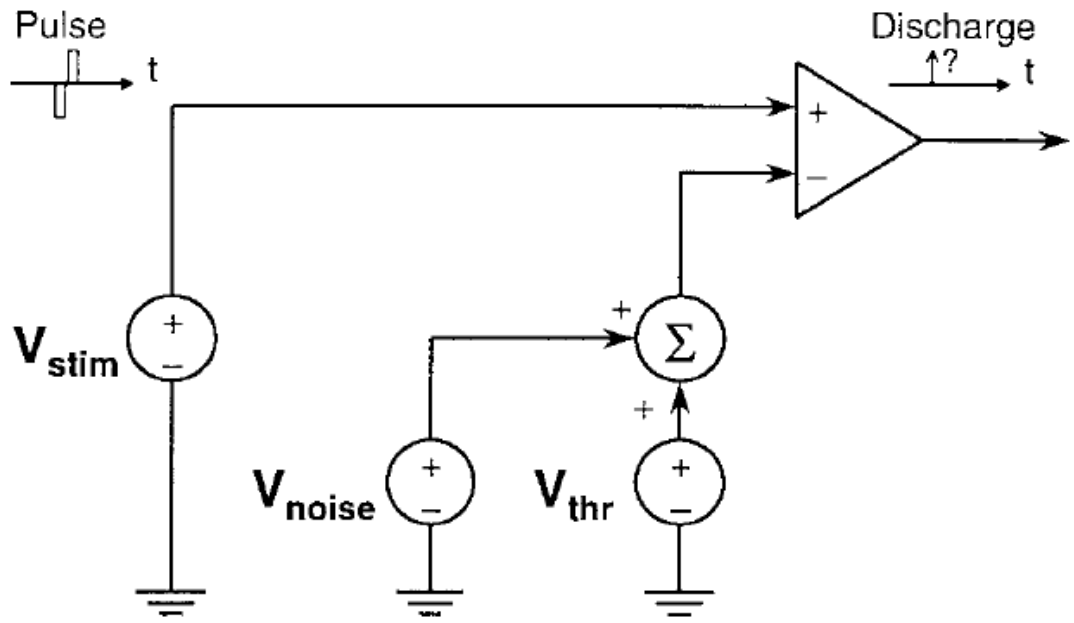

Fig. 2. Stochastic model of single-pulse response. See text for explanation of circuit components.

(from Bruce et al.,
IEEE TBME, 1999a)

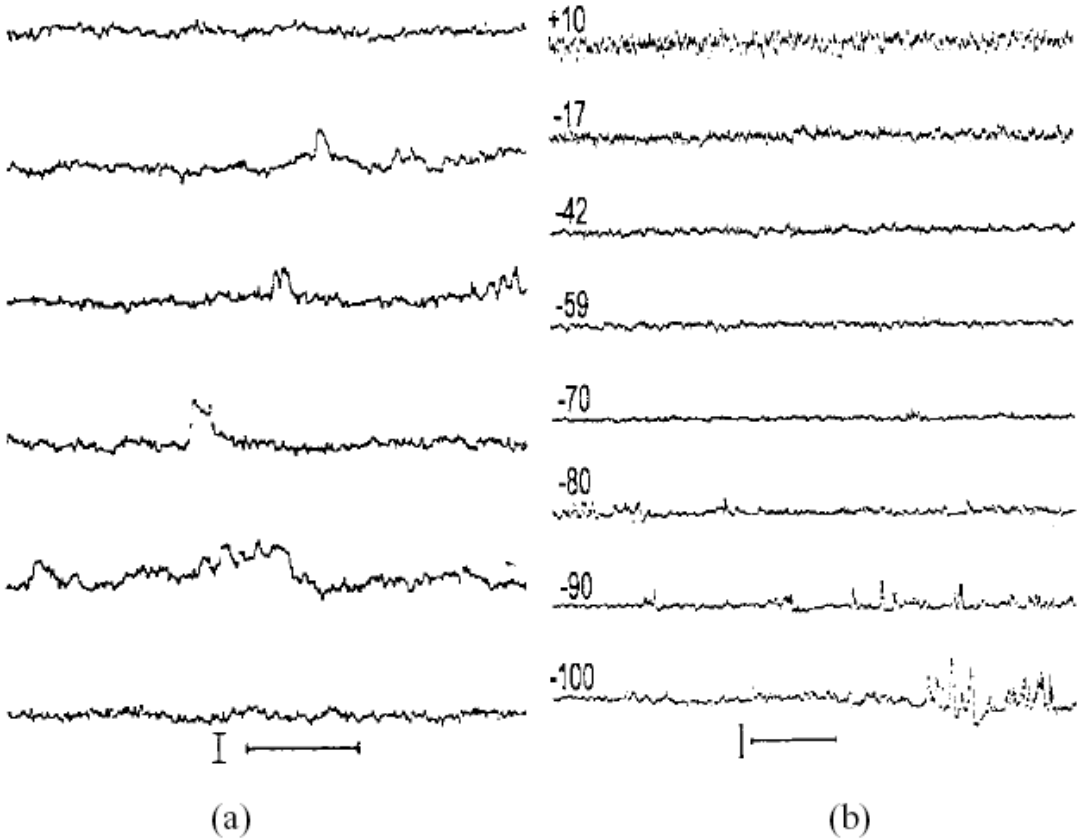

Fig. 1. Membrane-potential traces from [27] showing fluctuations in nerve fiber transmembrane potentials at the nodes of Ranvier. (a) Membrane potential traces at −90 mV. Horizontal scale: 10 ms; vertical scale: 1 mV. (Reprinted with permission from [27, Fig. 20] © 1968 IEEE.) (b) Membrane potential traces at different levels of membrane potential (given in mV above each trace). Horizontal scale: 1 ms; vertical scale: 5 mV. (Reprinted with permission from [27, Fig. 19] © 1968 IEEE.)

(from Bruce et al.,
IEEE TBME, 1999a)